Thermal analysis of high-bandwidth and energy-efficient 980 nm VCSELs with optimized quantum well gain peak-to-cavity resonance wavelength offset

Hui Li, Philip Wolf, Xiaowei Jia, James A. Lott, and Dieter Bimberg

View Online   Export Citation   CrossMark

ARTICLES YOU MAY BE INTERESTED IN

Relative intensity noise of temperature-stable, energy-efficient 980 nm VCSELs
AIP Advances **7**, 025107 (2017); https://doi.org/10.1063/1.4974258

Heat dissipation effect on modulation bandwidth of high-speed 850-nm VCSELs
Journal of Applied Physics **121**, 133105 (2017); https://doi.org/10.1063/1.4979532

Microwave extraction method of radiative recombination and photon lifetimes up to 85°C on 50 Gb/s oxide-vertical cavity surface emitting laser
Journal of Applied Physics **120**, 223103 (2016); https://doi.org/10.1063/1.4971978

Thermal analysis of high-bandwidth and energy-efficient 980 nm VCSELs with optimized quantum well gain peak-to-cavity resonance wavelength offset

Hui Li,[1,a)] Philip Wolf,[2] Xiaowei Jia,[1,3] James A. Lott,[2] and Dieter Bimberg[2,4]

[1]College of Mathematical and Physical Sciences, Qingdao University of Science and Technology, 266061 Qingdao, China
[2]Institut für Festkörperphysik and Zentrum für Nanophotonik, Technische Universität Berlin, Hardenbergstrasse 36, 10623 Berlin, Germany
[3]State Key Lab of Luminescence and Applications, Changchun Institute of Optics, Fine Mechanics and Physics, Chinese Academy of Sciences, 130033 Changchun, China
[4]King Abdul-Aziz University, 21589 Jeddah, Kingdom of Saudi Arabia

The static and dynamic performance of vertical-cavity surface-emitting lasers (VCSELs) used as light-sources for optical interconnects is highly influenced by temperature. We study the effect of temperature on the performance of high-speed energy-efficient 980 nm VCSELs with a peak wavelength of the quantum well offset to the wavelength of the fundamental longitudinal device cavity mode so that they are aligned at around 60 °C. A simple method to obtain the thermal resistance of the VCSELs as a function of ambient temperature is described, allowing us to extract the active region temperature and the temperature dependence of the dynamic and static parameters. At low bias currents, we can see an increase of the $-3\,\mathrm{dB}$ modulation bandwidth $f_{-3\mathrm{dB}}$ with increasing active region temperature, which is different from the classically known situation. From the detailed analysis of $f_{-3\mathrm{dB}}$ versus the active region temperature, we obtain a better understanding of the thermal limitations of VCSELs, giving a basis for next generation device designs with improved temperature stability. *Published by AIP Publishing.* https://doi.org/10.1063/1.5003288

Vertical-cavity surface-emitting lasers (VCSELs) are the typical light sources used for high-speed optical interconnects (OIs) for data communication based on multi-mode optical fibers. The goals for advanced VCSEL-based OIs include low energy consumption, low cost, efficient optical coupling, and large direct current modulation frequency.[1–3] The high bit rate, energy efficiency, and temperature stability of OIs are achieved by the direct current modulation of small oxide-aperture diameter VCSELs that are biased at moderate currents with simple non-return-to-zero on-off keying data coding.[4–6] Both the static and dynamic performance of VCSELs and OI systems are strongly influenced by an increase in the ambient temperature. In a VCSEL, a temperature increase can be caused by an ambient temperature increase and, more importantly, by the internal heating of the active region. Different approaches have been demonstrated to decrease the internal VCSEL temperature by, for example, a reduction of the thermal resistance, by minimizing the optical absorption, and by minimizing the series resistance.[7–9] The thermal resistance and temperature sensitivity of VCSELs are related to their structure and thermal conductivity of the constituent materials. The use of high thermal conductivity materials for the distributed Bragg reflector (DBR) mirrors and device layouts is helpful to achieve a high thermal performance for VCSELs.

Heat transport in semiconductor lasers can be simulated by numerically solving the heat conduction equation using finite-element methods.[10] The heat equation reads

$$\rho C \frac{\partial T}{\partial T} + \Delta \cdot (-k\Delta T) = Q, \tag{1}$$

where T (K) is the temperature, Q (W/m^3) is a heat source, ρ (kg/m^3) is the material density, C (J/kg·K) is the specific heat capacity, and k (W/m·K) is the thermal conductivity of the medium. The thermal behavior of semiconductor lasers is very complex, since many parameters are functions of temperature. The heat sources in VCSELs are more numerous than those in edge-emitting lasers, where the non-radiative recombination of charge carriers in the active region is the dominate heat source. The important heat sources in VCSELs are non-radiative recombination, reabsorption of spontaneous emission in the active region, and Joule heating. The heat flux distribution in the device is related to the voltage drop across the active region and the DBRs.[11] The voltage drop across the active region is $\sim$1.26 V for 980 nm VCSELs (as estimated from the real-space bandgap energy). The voltage drop across the DBRs is caused by interface barriers, which increase the resistance and the threshold voltage.[12] The heat transfer equation is solved by defining an initial constant value of temperature T_0 for all VCSEL materials.

The device structure of our VCSELs used in this work is described in detail in Ref. 13. This structure employs a -15 nm room temperature quantum well (QW) gain peak wavelength [based on a room temperature photoluminescence (PL) measurement of a QW active region calibration sample] to etalon wavelength offset to improve our VCSELs' elevated temperature static and dynamic performance.[14] A contour plot of the temperature distribution in a cross-sectional plane (r-z plane) of, for example, a 2.5 μm

a)Electronic mail: lihui6526@qust.edu.cn

oxide-aperture diameter 980 nm VCSEL is given in Fig. 1. The continuous wave (CW) injection current is 1 mA, the voltage is 2.064 V, and the output power is 0.233 mW. The total dissipated heat in the VCSEL is 1.831 mW. Based on the voltage drop across the active region and DBRs, the active region heat source is calculated to be 4.02×10^{15} W/m^3. So, 1 mA of CW injection current causes the active region temperature to increase by 3.427 °C.

The simulation results are just as expected. The active region temperature is much higher than the ambient temperature. Since the static and high-speed modulation performance of VCSELs is decisively influenced by the active region temperature, an accurate knowledge of the heat generation inside the device is required. A precise determination of the active region temperature T_{active} is very important for a good understanding of the device and to provide insight for the next generation of device designs. A common method to obtain $T_{internal}$ is the determination of the thermal resistance from the emission spectra. According to Ref. 15, the thermal resistance R_{th} can be determined from $R_{th} = (\Delta\lambda/\Delta P_{diss})/(\Delta\lambda/\Delta T)$. From the fundamental mode peak emission wavelength, we determine the cavity resonance wavelength shift rate versus the dissipated power $\Delta\lambda/\Delta P_{diss}$, where $P_{diss} = I \times V - P_{out}$, and the heat-sink temperature variation is $(\Delta\lambda/\Delta T)$. Then, we can calculate the thermal resistance. This is an approximate approach, as we ignore the bias current effect on the internal heating upon obtaining $\Delta\lambda/\Delta T$. The thermal resistance can be more precisely calculated from $R_{th} = \Delta T/\Delta P_{diss}$, which relates the average temperature change ΔT in the laser cavity to a change ΔP_{diss} of the dissipated power. For this purpose, the VCSEL is typically driven with electrical pulses up to a few hundred nanoseconds, which are shorter than the thermal time constant which is in the range of some microseconds. With this method, no internal heating of the VCSEL by the dissipated power arises and thereby no thermal wavelength shift appears. In this work, we determine the cold cavity peak wavelength by linearly extrapolating the peak wavelength change with the CW dissipated power emission wavelength λ_0 of the fundamental mode to the point of no internal heating at $P_{diss} = 0$ mW. We start with emission spectra measurements at different bias currents at an ambient temperature $T_{ambient} = 25$ °C using our 2.5 µm oxide-aperture diameter 980 nm VCSELs, from which we extract the fundamental mode peak emission wavelength. For each bias
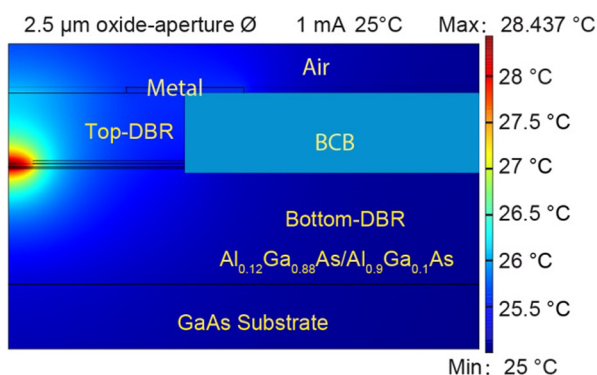

FIG. 2. The measured fundamental mode peak emission wavelength λ_P versus the CW dissipated electrical power P_{diss} for different ambient temperatures $T_{ambient}$ for 980 nm VCSELs. The points marked with circles are the extrapolated wavelengths λ_0 of the fundamental mode peak emission wavelengths without internal heating where $P_{diss} = 0$ mW at the given ambient temperature.

current, we calculate the dissipated power via $P_{diss} = I \times V - P_{out}$. Then, we plot the fundamental mode peak emission wavelength change versus the dissipated power. By using simple linear extrapolation, we identify the peak emission wavelength λ_0 of the fundamental mode without internal heating at $P_{diss} = 0$ mW. This extrapolated cold cavity wavelength from a CW measurement is identical to a measurement of the peak wavelength in pulsed operation. We repeat this procedure for different temperatures $T_{ambient}$, resulting in the plot in Fig. 2 to determine the ambient temperature dependence of the active region and extract the λ_0 values at different ambient temperatures, as shown in Fig. 3. We can easily see that λ_0 linearly increases with ambient temperature with a slope of 0.065 nm/K, as shown in Fig. 3. This analysis gives us accurate values of the cavity resonance wavelength shift rate versus the heat-sink temperature $\Delta\lambda/\Delta T$.

As can be seen in Fig. 2, at all investigated ambient temperatures $T_{ambient}$, the fundamental mode peak emission wavelength λ_P increases linearly with the dissipated electrical power P_{diss} but with different slopes. No curvature is seen even for high dissipated power P_{diss}. The slope of the λ_P versus P_{diss} curve is given by the cavity resonance

FIG. 1. The simulated temperature distribution T(r,z) of our 2.5 µm oxide-aperture diameter 980 nm VCSELs at a continuous wave (CW) bias current of 1 mA.
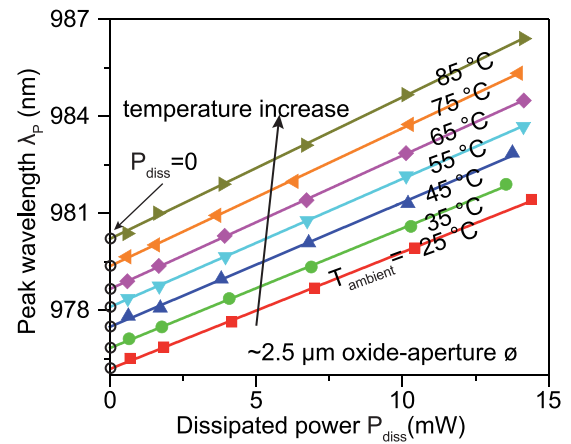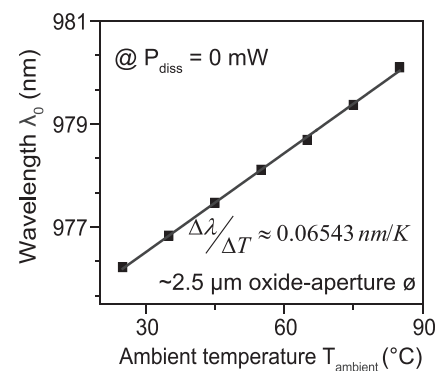

FIG. 3. The wavelength λ_0 of the fundamental mode peak emission wavelength without internal heating at $P_{diss} = 0$ mW, determined by simple linear extrapolation for different ambient temperatures $T_{ambient}$ from the data in Fig. 2. The slope (0.06543 nm/K) of the linear fit gives the value of the cavity resonance wavelength shift rate versus temperature $\Delta\lambda/\Delta T$.

wavelength shift rate versus dissipated power $\Delta\lambda/\Delta P_{diss}$, which varies for each given ambient temperature. At ambient temperatures $T_{ambient}$ of 25, 35, 45, 55, 65, 75, and 85 °C, the cavity resonance wavelength shift rate versus dissipated power $\Delta\lambda/\Delta P_{diss}$ is 0.360, 0.369, 0.385, 0.396, 0.412, 0.426, and 0.440 nm/mW, respectively. These data allow us to derive the dependence of the thermal resistance on the ambient temperature. We can calculate now the thermal resistance using $R_{th} = (\Delta\lambda/\Delta P_{diss})/(\Delta\lambda/\Delta T)$. The extracted values of R_{th} are shown in Table I. The high thermal resistance of our small oxide-aperture diameter VCSELs results in large active region temperatures and negatively impacts the high-speed modulation performance. By using our ambient temperature-dependent thermal resistance data, we can perform a basic thermal effects analysis based on the VCSEL's active region temperature at different bias currents.

From the ambient-temperature-dependent thermal resistance, we extract the active region temperature T_{active} for each point in a given set of L-I-V curves within the linear L-I regions. The active region temperature T_{active} change with increasing bias current can be estimated for the linear L-I region using $T_{active} = T_{ambient} + R_{th} \times (I \times V - P_{out})$.[15] This gives us the possibility to perform a detailed analysis of the thermal effects and extract the internal temperature-dependent VCSEL parameters. Furthermore, we can exclude the influence of internal heating in the examination of the L-I-V curves. By measuring the L-I-V curves at certain ambient temperatures, we obtain the output powers at certain currents (for example, at 1 mA). We can next calculate the active region temperatures by repeating this procedure at other ambient temperatures. Finally, the optical output power P_{out} as a function of T_{active} for each individual bias current can be determined, as shown in Fig. 4. Usually, the optical output power decreases with increasing T_{active}. Instead, our VCSELs show a clear first increase in optical output power with increasing active region temperature T_{active}. The P_{out} reaches a maximum as T_{active} increases but then P_{out} decreases with further increases in T_{active}. This is due to our VCSEL design where the peak PL gain from our quantum well active region is offset from the cavity resonance wavelength by about -15 nm. This offset improves our VCSELs' high temperature performance in both static and high-speed modulation operations.

Figure 5 shows the -3 dB modulation bandwidth f_{-3dB} change with the active region temperature T_{active} at different bias currents. At low bias currents, we can see an increase of f_{-3dB} with increasing internal active region temperature,
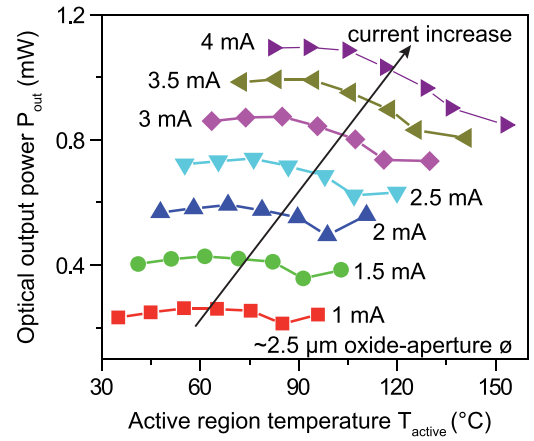

FIG. 4. Output power of the 2.5 μm oxide-aperture diameter VCSEL versus the active region temperature T_{active} for different bias currents.

which is contrary to typical VCSEL behavior. Again, this increase in f_{-3dB} is a result of the -15 nm gain peak-to-cavity wavelength offset, which leads to a partial increase of the differential gain with an increase in the active region temperature. With an increase in the bias current, we find that thermal effects mainly limit the bandwidth. At currents larger than 2.4 mA and an active region temperature larger than 95 °C, the -3 dB bandwidth shows no increase with increasing bias current. This means that the modulation bandwidth is limited thermally at large currents. Improving the heat dissipation by, for example, using novel VCSEL packaging methods will lead to further improvement of the modulation bandwidth $f_{-3\,dB}$ at large bias.

In conclusion, we studied numerically and experimentally thermal effects on the device performance of high-speed energy-efficient VCSELs with an optimized quantum well PL peak-to-cavity wavelength offset. We used a simple model to obtain the VCSEL thermal resistance. The ambient temperature-dependent thermal resistance in-turn enables us to extract the internal active region temperature versus bias current. A detailed analysis of the thermal effects allows us to extract the temperature dependence of the internal VCSEL parameters. From the modulation bandwidth f_{-3dB} versus the internal active region temperature, we gain insight
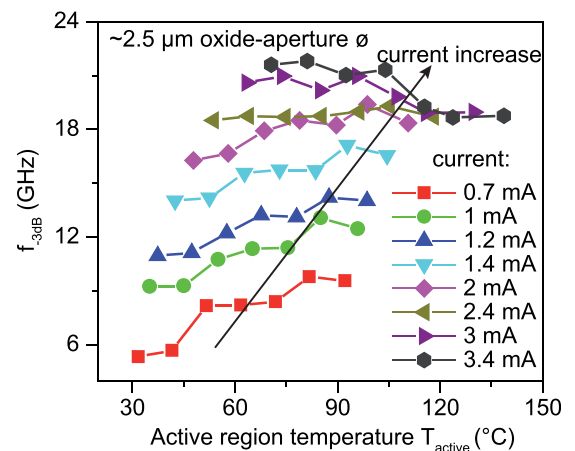
TABLE I. Thermal resistance R_{th} for 2.5 μm oxide-aperture diameter 980 nm VCSELs at different ambient temperatures.

Ambient temperature (°C)	Thermal resistance R_{th} (K/mW)
25	5.496
35	5.643
45	5.878
55	6.05
65	6.29
75	6.51
85	6.72

FIG. 5. -3 dB small signal modulation bandwidth of the 2.5 μm oxide-aperture diameter VCSEL versus the extracted active region temperature T_{active} for different bias currents.

into the thermal limitations of our high-speed VCSELs. This information is extremely useful for improving the device designs of our next generation VCSELs to achieve further improved temperature stability.

[1]A. Larsson, "Advances in VCSELs for communication and sensing," IEEE J. Sel. Top. Quantum Electron. **17**(6), 1552–1567 (2011).

[2]A. Kasukawa, "VCSEL technology for green optical interconnects," IEEE Photonics J. **4**(2), 642–646 (2012).

[3]D. Bimberg, A. Larsson, and A. Joel, "Faster, more frugal, greener VCSELs," Compd. Semicond. **22**, 34–39 (2014).

[4]P. Moser, P. Wolf, G. Larisch, H. Li, J. A. Lott, and D. Bimberg, "Energy-efficient oxide-confined high-speed VCSELs for optical interconnects," Proc. SPIE **9001**, 900103 (2014).

[5]H. Li, P. Wolf, P. Moser, G. Larisch, A. Mutig, J. A. Lott, and D. Bimberg, "Energy-efficient and temperature-stable 980 nm VCSELs for 35 Gb/s error-free data transmission at 85 °C with 139 fJ/bit dissipated heat," IEEE Photonics Technol. Lett. **26**(23), 2349–2352 (2014).

[6]E. Haglund, P. Westbergh, J. S. Gustavsson, E. P. Haglund, A. Larsson, M. Geen, and A. Joel, "30 GHz bandwidth 850 nm VCSEL with sub-100 fJ/bit energy dissipation at 25–50 Gbit/s," Electron. Lett. **51**(14), 1096–1098 (2015).

[7]A. Al-Omari and K. Lear, "VCSEL with a self-aligned contact and copper-plated heatsink," IEEE Photonics Technol. Lett. **17**(9), 1767–1769 (2005).

[8]D. Mathine, H. Nejad, D. Allee, R. Droopad, and G. Maracas, "Reduction of the thermal impedance of vertical-cavity surface-emitting lasers after integration with copper substrates," Appl. Phys. Lett. **69**(4), 463–464 (1996).

[9]K. L. Lear and R. P. Schneider, Jr., "Uniparabolic mirror grating for vertical cavity surface emitting lasers," Appl. Phys. Lett. **67**(5), 605–607 (1996).

[10]R. Mehandru, G. Dang, S. Kim, F. Ren, W. S. Hobson, J. Lopata, S. J. Peartonc, W. Changd, and H. Shen, "Finite difference analysis of thermal characteristics of CW operation 850 nm lateral current injection and implant-apertured VCSEL with flip–chip bonding design," Solid State Electron. **46**, 699–704 (2002).

[11]C. Webb and J. Julian, "Handbook of laser technology and applications: Laser design and laser systems," in *Vertical-Cavity Surface-Emitting Lasers* (CRC Press, Boca Raton, FL, USA, 2004), pp. 673–688.

[12]J. Piprek, "Electro-thermal analysis of oxide-confined vertical-cavity lasers," Phys. Status Solidi (a) **188**(3), 905–912 (2001).

[13]H. Li, P. Wolf, P. Moser, G. Larisch, J. A. Lott, and D. Bimberg, "Temperature-stable, energy-efficient and high-speed oxide-confined 980 nm VCSELs for optical interconnects," IEEE J. Sel. Top. Quantum Electron. **21**(6), 405–413 (2015).

[14]H. Li, P. Wolf, P. Moser, G. Larisch, A. Mutig, J. A. Lott, and D. Bimberg, "Impact of the quantum well gain-to-cavity etalon wavelength offset on the high temperature performance of high bit rate 980 nm VCSELs," IEEE J. Quantum Electron. **50**(8), 613–621 (2014).

[15]R. Michalzik, "VCSEL fundamentals," in *VCSELs: Fundamentals, Technology and Applications of Vertical-Cavity Surface-Emitting Lasers*, edited by R. Michalzik (Springer-Verlag, Berlin, Germany, 2013), vol. 166, pp. 19–75.